Articles

Compositionally Induced Phase Transitions and Nonlinear Optic Response in $ABCO_4$ Crystal Solution Phases $ALiPO_4$ (A = Sr, Ba, Pb)

Cheryl S. Liang, Hellmut Eckert,* Thurman E. Gier, and Galen D. Stucky*

Department of Chemistry, University of California at Santa Barbara, Santa Barbara, California 93106

Received May 19, 1992. Revised Manuscript Received February 12, 1993

Potentially useful second harmonic generating (SHG) compounds with the stoichiometry $A_xA'_{1-x}LiPO_4$ (A, A' = Sr, Ba, Pb) have been prepared. Their structural and optical properties are characterized by X-ray powder diffraction, vis/UV spectroscopy, SHG measurements, ^{31}P magic angle spinning (MAS) NMR, and Raman spectroscopy. $BaLiPO_4$ is orthorhombic (ortho I); a = 8.633(7) Å, b = 8.735(5) Å, and c = 5.211(4) Å. $SrLiPO_4$ is hexagonal; $a = b$ = 5.002(1) Å and c = 8.209(2) Å. The regions of solid–solid solubility for these phases upon mutual cation substitution are defined by XRD, SHG measurements, and ^{31}P MAS NMR. ^{31}P isotropic chemical shifts are shown to be sensitive to cation distribution effects and to structural phase changes. ^{31}P MAS NMR spectroscopy also shows that for both pure $BaLiPO_4$ and $SrLiPO_4$ there is only one crystallographically distinct phosphorus site. SHG intensities are maximized by bringing the solid-state solution phases close to structural phase transitions, with changes of more than an order of magnitude from the SHG responses of either of the pure phases.

Introduction

Materials with nonlinear optical properties are important for many technological applications, such as second harmonic generation (SHG), optical switching, and wave guides for optical transmission. So far a few useful nonlinear optic (NLO) crystals such as $KTiOPO_4$ (KTP), $LiNbO_3$, and KH_2PO_4 (KDP) have been utilized for laser frequency conversion in the visible region and near-UV region. Materials with high second harmonic generating efficiency as well as absorption edge lower than KTP (350 nm) are necessary due to the demand for high resolution data storage and processing, using diode and short wavelength lasers. Currently, β-BaB_2O_4 is the most widely used UV transparent frequency doubling crystal with a powder SHG of about 80 times that of quartz and an absorption edge around 200 nm.[1,2] Since it is transparent in the UV region, this also makes third and higher harmonic generation feasible, using primary wavelengths ≥800 nm.

From a thermodynamic–macroscopic point of view, Miller[3] proposed that the SHG coefficient, $d_{ijk}^{(\omega)}$ in crystals are related to the linear susceptibility, χ_{ii} by

$$d_{ijk}^{(\omega)} = \chi_{ii}^{(\omega)} \cdot \chi_{jj}^{(\omega)} \cdot \chi_{kk}(0) \cdot \Delta_{ijk}^{(2\omega)} \qquad (1)$$

where $\chi_{jj} = (n^2_{jj} - 1)/4\pi$ is the linear polarization (α), n is the index of refraction; $\Delta_{ijk}^{(2\omega)}$ is Miller's coefficient with $\Delta_{ijk}^{(2\omega)} = -1/2(m_e/e^3)N_e k_a$ and m_e the electronic mass; N_e the number of electrons per unit volume; and k_a the anharmonic force constant; which is determined by potential well anisotropy. From the above equation, Miller has demonstrated that it is possible to predict the SHG of many materials with simple geometries.[3] Bergman et al.[4] and Levine[5] have further related the macroscopic polarization and SHG to localized bond polarizabilities by summing over all the different bond orientations and tensor components:

$$d_{ijk}^{(\omega)} \propto \sum_{\substack{IJK \\ \text{all bonds}}} a_{iI} a_{jJ} a_{kK} \beta_{IJK} \qquad (2)$$

where a_{rR} ($r = i, j, k$; $R = I, J, K$) is a second-rank tensor which describes the orientation and β_{IJK} is third-rank tensor which is defined by the second-order bond polarization.

The oxygen anion has a strikingly different polarization response in ferroelectrics than other lower dielectric oxides.[6,7] Biltz, Tessmann, and Bussman studied the oxygen linear polarizabilities (α) as a function of the crystal lattice and found that while a fixed polarizability is sufficient to describe most ions investigated, the polarization of the O^{2-} ion depends linearly on the volume per O^{2-} (V). In spinels and ferroelectric oxides, the anisotropy of O^{2-} is greater, and α is proportional to V^n with n varying from 1 to 4.[7,8,22] This, along with Miller's relationship,

* Authors for correspondence.

(1) Eimerl, D.; Davis, L.; Velsko, S. *J. Appl. Phys.* **1987**, *62*, 1968.
(2) Chen, C.; Wu, B.; Jiang, A.; You, G. *Sci. Sinica (Ser. B)* **1985**, *28*, 235.
(3) Miller, R. C. *Appl. Phys. Lett.* **1964**, *5*, 17.
(4) (a) Bergman, J. G.; Crane, G. R. *J. Chem. Phys.* **1974**, *60*, 2470. (b) Tofield, B. C.; Crane, G. R.; Bergman, J. G. *Trans. Faraday Soc.* **1974**, *2*, 1488. (c) Bergman, J. G.; Crane, G. R. *J. Solid State Chem.* **1975**, *12*, 172.
(5) (a) Levine, B. F. *Phys. Rev. Lett.* **1969**, *22*, 787. (b) Levine, B. F. *Phys. Rev. Lett.* **1970**, *25*, 440. (c) Levine, B. F. *Phys. Rev. B* **1973**, *7*, 2600.
(6) Biltz, H.; Klemm, W. In *Raumchemie d. festen Stoffe*; Verlag L. Voss: Leipzig, 1934.
(7) Biltz, H.; Benedek, G.; Bussmann-Holder, A. *Phys. Rev. B* **1987**, *35*, 4840.

0897-4756/93/2805-0597$04.00/0

offers the opportunity to structurally design NLO properties by varying the potential anharmonicity (k_a) and the effective oxygen volume (V).

At the microscopic level, it is known that excitation of the lattice vibration modes in Raman spectroscopy produces fluctuations in the optic dielectric constant at that frequency provided the excited mode has suitable symmetry, since the processes for Raman active modes are the same as those responsible for the electrooptic effect.[8] This effect has been demonstrated by Johnston et al.[9] for the GaAs system where for the transverse optic mode ω_T

$$d\chi_{ij}(\omega_0)/dQ_k = \partial\chi_{ij}(\omega_0)/\partial Q_k = \alpha_{ij,k} \quad (3)$$

where $|d\chi_{ij}(\omega_0)/dQ_k|^2$ is proportional to the intensity of a side band; Q_k is the thermal excited displacement; $\alpha_{ij,k}$ is the nonvanishing term of linear polarizability tensor which is proportional to the first order susceptibility χ_{ijk}; and for the longitudinal optic mode ω_L

$$\frac{d\chi_{ij}(\omega_0)}{dQ_k} = \left(\frac{\partial\chi(\omega_0)}{\partial Q_k}\right)_{E=0} + \left(\frac{\partial\chi(\omega_0)}{\partial E(\omega_L)}\right)_{Q=0}\frac{1}{\partial Q_k/\partial E(\omega_L)} = \alpha_{ij,k} + \frac{\xi_{ijk}}{\beta_{kk}(\omega_L)} \quad (4)$$

where $d\chi_{ij}(\omega_0)/dQ_k$ is equal to the linear polarizability plus a constant. Also, from the Lyddane–Sachs–Teller (LST) relation

$$\omega_T^2/\omega_L^2 = \epsilon(\infty)/\epsilon(0) \quad (5)$$

where the static dielectric constant, $\epsilon(0)$, is also proportional to the linear polarization, $\epsilon(0)$ increases when the transverse optical phonon frequency, ω_T, decreases. Therefore, when applying an electric field to a system near structural phase transitions the restoring force decreases due to low values of ω_T and consequently increases the SHG response. This phenomenon has been well demonstrated in $BaTiO_3$.[10-12]

The above considerations formulate a simple recipe for tuning the SHG in inorganic oxides. By introducing the combination of a large and small cation in a ternary metal oxide, we expect to increase the anharmonicity at the oxygen atom sites, the polarizability, and concurrently the SHG. In addition, structural instabilities near phase transitions, or introduced by creating solid-state solutions near pure phase compositions can be expected to introduce the lattice stress and phonon modes necessary to generate greater polarization susceptibilities. Ternary metal oxides with the $ABCO_4$ stoichiometry appear particularly suitable for this purpose.

The $ABCO_4$ structure is typified by the $BaAl_2O_4$ structure (stuffed tridymite) which is hexagonal with a close packed oxygen lattice with one large 8–9-coordinate ion and two small 4-coordinate ions for every four oxygen atoms.[13] Depending on the particular cation arrangement, the basic structure and most of its derivatives are noncentrosymmetric. The high tridymite structure consists of tetrahedral SiO_4 units which are linked together through corner sharing of all four oxygen atoms of each tetrahedron, thereby creating a one dimensional six-ring channel. The six membered ring is made up of alternating up (U) and down (D) tetrahedra, UDUDUD. The most symmetrical linkage of tetrahedra is in the high-temperature form which belongs to the hexagonal $P6_3$ space group with empty channels. Therefore, the stuffed tridymite structure can be considered an open framework structure constituting the "host" and a large cation introduced into these channels as the "guest". The open framework architecture and the soft potentials associated with the corner-shared tetrahedra present in this structure generates numerous structural phases that are energetically comparable.

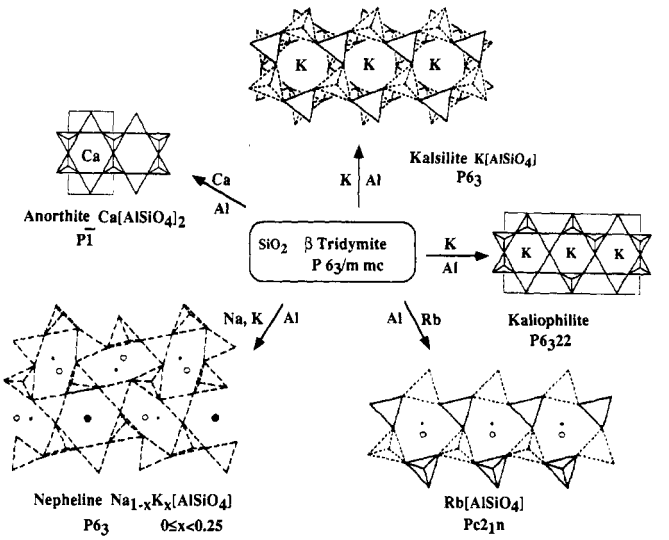

Figure 1. Tridymite structure stuffed with various cations. The structure drawings (from Liebau, F. *Structural Chemistry of Silicates*; Springer-Verlag: Berlin, 1985) illustrate different tetrahedral arrangements and distortions through tilting of the tetrahedra linkage.

Part or all of the Si^{4+} ions in the tridymite structure can be replaced by M^{n+} species where M is a cation with $n \leq 3$ and has tetrahedral coordination. The loss of valence charge is balanced by addition of other metal atoms to the structure. Depending on the size of the charge-balancing cation in the channel, the six membered ring is able to distort through geometrical changes in the tetrahedra, which can either be tilted or rearranged in their orientation of up or down around the ring plane in order to increase or decrease the ring size to better accommodate the cation. This host/guest relationship of inclusion chemistry can be used to introduce large asymmetry into the framework. Figure 1 shows different cation substitution models of stuffed tridymite. Using the above argument, there are two ways to create large asymmetry in the stuffed tridymite structure; by introducing a large cation into the channel, or by introducing cations of different sizes into the channel structure. Figure 1 illustrates an example where both sodium and potassium atoms are included in the channels, with each cation inducing a different distortion into the six-membered ring.

Accordingly, we have synthesized over 200 $ABCO_4$ compounds with selected examples given in Table I. Some of these materials indeed have large SHG responses relative to quartz, and modification of their composition does lead to structural and SHG changes. In the present paper we

(8) Tessmann, G. R.; Kahn, A. H.; Shockley, W. *Phys. Rev.* **1953**, *92*, 890.
(9) Kaminow, I. P. *Ferroelectricity*; Weller, E. F., Ed.; Elsevier: Amsterdam, 1967.
(10) Johnston, W. D., Jr. *Phys. Rev. B.* **1970**, *1*, 3494.
(11) Baeuerle, D.; Genzel, L.; Martin, T. P. *Phys. Status Solidi B* **1973**, *59*, 459.
(12) Kittel, C. *Introduction to Solid State Physics*, 6th ed.; Wiley: New York, 1986.
(13) Inoue, K. *Ferroelectrics* **1983**, *52*, 253.

Table I. SHG Measured Relative to Quartz for Some Potentially UV-Transparent $ABCO_4$ Materials[a]

material	SHG (±10%)	material	SHG (±10%)
$Ba_{0.55}Pb_{0.45}LiPO_4$	486	$KLiCrO_4$	23
$Pb_{0.9}Sr_{0.1}BeSiO_4$	233	$RbLiMoO_4$	23
$PbBeSrO_4$	200	$BaZnSiO_4$	14
$Pb_{0.95}Ba_{0.05}BeSiO_4$	166	$BaZnGeO_4$	13
$SrLiVO_4$	135	$KLiSeO_4$	11
$PbAl_2O_4$	133	$LaZnGaO_4$	10
$Ba_{0.49}Pb_{0.4}Sr_{0.11}LiPO_4$	133	$BaLiPO_4$	10
$Sr_{0.925}Pb_{0.075}LiPO_4$	120	$SrLiPO_4$	9
$TlZnPO_4$	114	$PbBeGeO_4$	9
$Ba_{0.35}Sr_{0.35}Pb_{0.3}LiPO_4$	100	$BaLiPO_4$	9
$Ba_{0.9}Sr_{0.1}LiPO_4$	81	$RbZnPO_4$	8
$PbLiPO_4$	37	$TlBePO_4$	5
$PbZnSiO_4$	25	$CsZnAsO_4$	4

[a] The currently commercially available β-BaB_2O_4 has a powder SHG of 80 times quartz.

show that the SHG for $ABCO_4$ compounds can be increased substantially by choosing compositions near structural phase transitions. Similar *linear* polarization phenomena have been demonstrated for ferroelectric systems such as $KNbO_3$ and $KTaO_3$, where the dielectric constant increases by two orders of magnitude as the composition approaches a phase transition from either the Ta or Nb side.[14]

Experimental Section

Synthesis and Characterization. $Sr_xPb_{1-x}LiPO_4$, $Ba_xPb_{1-x}LiPO_4$, and $Ba_xSr_{1-x}LiPO_4$ ($0 \le x \le 1$) solid solutions were synthesized using the following procedure. Stoichiometric amounts of $SrCO_3$ (Aldrich, 98+%), $BaCO_3$ (Fisher, reagent grade) PbO (Fisher, reagent grade), Li_2CO_3 (Fisher, redried at 500 °C for 20 h), and $NH_4H_2PO_4$ (Fisher, reagent grade) were mixed in a platinum crucible and slowly heated from 200 to 800 °C to drive off CO_2, NH_4OH, and H_2O, then thoroughly ground and fired between 900 and 1000 °C. The samples were subsequently quenched on aluminum plates to room temperature. For compounds near their structural phase transition, the above cooling technique becomes inadequate since it results in two-phase materials. These samples were either quenched in liquid nitrogen or cooled slowly to room temperature at 10 °C/h. All compounds were characterized by X-ray powder diffraction and indexed using Scintag diffractometer software.

Optical and Spectroscopic Analysis. The second harmonic generation (SHG) efficiencies relative to α-quartz were measured on powders (particle sizes 1–3 μm) using an apparatus similar to Dougherty and Kurtz[15] in reflection mode with samples loaded in capillaries of 1 mm inner diameter. A Q switched pulsed Nd:YAG laser operating at 1064 nm was used with pulse-to-pulse variation of 5%. The apparatus has an attenuator to control the laser power output and a monochromator to further filter out spurious light. It is also equipped with a fast oscilloscope (Tektronix 2467B 400MHz) which is capable of acquiring waveforms at a time resolution of 2 ns.

A total of 10 measurements/sample were made, each measurement being averaged over 20 traces at 2-Hz repetition rate. The standard deviation between average traces was less than 5%. All SHG intensities were measured and referenced in the same way as the quartz standard.

Vis/UV reflectance spectra using $MgCO_3$ as a standard were obtained from a computerized Cary 14 vis/UV spectrometer operating in the wavelength range 220–850 nm. Reported absorption edges are the inflection point of the spectra. IR data were collected on a Bio-rad FTS-60 FTIR spectrometer using diffuse reflectance apparatus supplied by Spectra Tech Inc. and Kubelka-Munk function was applied to all spectra. Raman spectra were collected on an Instruments SA U1000 spectrometer equipped with an argon 514-nm continuous-wave ion laser.

(14) Perrotta, A. J.; Smith, J. V. *Mineral Mag.* **1965**, *35*, 588.
(15) Triebwasser, S. *Phys. Rev.* **1959**, *114*, 63.

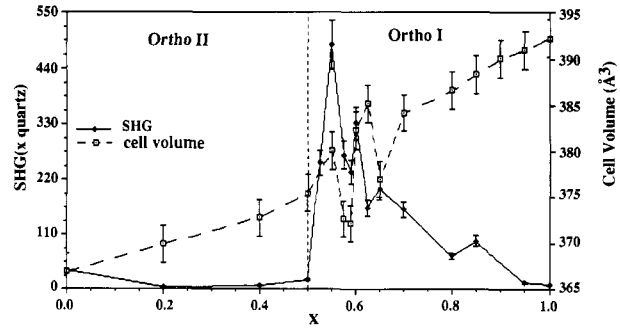

Figure 2. Plots of SHG (♦) and cell volume (⊡) vs x for $Ba_xPb_{1-x}LiPO_4$. The highest SHG is 486 times that of quartz for the composition $Ba_{0.55}Pb_{0.45}LiPO_4$ and the second highest SHG is 332 for $Ba_{0.6}Pb_{0.4}LiPO_4$.

Solid-state ^{31}P NMR spectra were obtained on a General Electric GN-300 widebore system operating at 121.65 MHz, equipped with a high-power magic angle spinning probe from Chemagnetics. Samples were loaded in 9.5-mm-o.d. Kel-F spinners and spun at speeds between 0.0 and 3.2 kHz. Standard single-pulse acquisition was utilized with a 7-μs 90° pulse length and recycle delays of 10 s. All samples are referenced to external 85% H_3PO_4 (downfield shifts positive).

Measurements of the ^{31}P chemical shift tensor components were difficult for these systems due to very small anisotropies. Even static spectra showed negligible anisotropy confirming the approximately tetrahedral symmetry of the phosphorus atoms.

Results and Discussion

Structures. $Ba_xPb_{1-x}LiPO_4$: It has been reported by Elammari et al. that $PbLiPO_4$ is orthorhombic (designated here as the orthorhombic II phase) with space group $Pna2_1$; $a = 7.969(3)$ Å, $b = 18.591(5)$ Å, and $c = 4.926(1)$ Å.[16] From X-ray powder diffraction data, we have determined that $BaLiPO_4$ is also orthorhombic (orthorhombic I); $a = 8.633(7)$ Å, $b = 8.735(5)$ Å, and $c = 5.211(4)$ Å. The ^{31}P MAS NMR spectrum shows of a single peak at 3.0 ppm confirming that there is only one crystallographic unique phosphorus atom per unit cell. In the solid–solution system $Ba_xPb_{1-x}LiPO_4$ a structural phase transition occurs at $x = 0.5$. Figure 2 indicates Vegard-type behavior showing that the cell volume increases with x. The largest deviation in cell volume in Figure 2, with reproducible values from replicate syntheses, is found near the structural phase transition. The largest deviation from Vegard's plot occurs between $0.65 \le x \le 0.55$ (Figure 2). This is significant because the SHG intensities also attain maximum values in this composition range.

$Sr_xPb_{1-x}LiPO_4$: Pure $SrLiPO_4$ phase is hexagonal with lattice constants $a = b = 5.002(1)$ Å, and $c = 8.209(2)$ Å. This structure can only accept trace amount of lead (<1% Pb). Upon higher lead doping, an orthorhombic structure appears. The X-ray powder diffraction and ^{31}P MAS NMR data suggest that this phase is similar to that of $BaLiPO_4$ (ortho I) with only one crystallographically unique phosphorus atom. This phase is stable for contents of $0.99 \ge x \ge 0.90$; higher substitution of lead results in the $PbLiPO_4$ (ortho II) structure (see Figure 3). In these figures the cell volume of $SrLiPO_4$ has been doubled to facilitate a comparison with the orthorhombic structures which have about twice the cell volume of that of the hexagonal phase.

$Ba_xSr_{1-x}LiPO_4$: Figure 4 shows a Vegard's plot for the system $Ba_xSr_{1-x}LiPO_4$ revealing a structural phase transition near $x = 0.5$. Once again the cell volumes of the

(16) Dougherty, J. P.; Kurtz, S. K. *J. Appl. Crystallogr.* **1976**, *9*, 145.

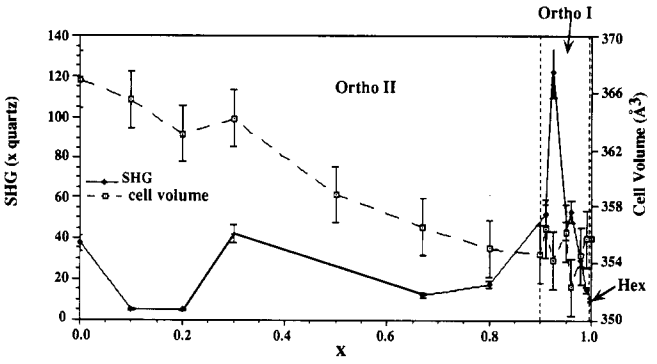

Figure 3. Plot of SHG (♦) and cell volume (⊡) vs x for $Sr_xPb_{1-x}LiPO_4$. The highest SHG is 122 times that of quartz for the composition $Sr_{0.925}Pb_{0.075}LiPO_4$.

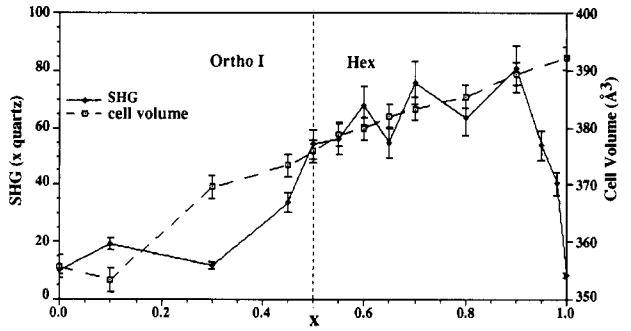

Figure 4. Plot of SHG (♦) and cell volume (⊡) vs x for $Ba_xSr_{1-x}LiPO_4$. The highest SHG is 80 times quartz for the composition $Ba_{0.9}Sr_{0.1}LiPO_4$.

hexagonal phase have been doubled for convenience in graphing. Compounds with $x = 0.55$, 0.575, 0.6, and 0.65 can be prepared hexagonal but transform to the orthorhombic structure after several months at room temperature. This suggests that at high temperature both hexagonal and orthorhombic phases coexist and upon fast cooling these phases are locked into the structure so that we obtain mixed phase materials at room temperature. However, upon slow cooling the structure in the orthorhombic phase transforms to a hexagonal geometry and there exists a phase transition in which the atoms rearrange themselves into the most stable orthorhombic phase. This suggests that the phase transition from hexagonal to orthorhombic I (and vice versa) is a displacive transition, i.e., the atoms merely rearrange themselves without breaking bonds.

^{31}P NMR Results. $PbLiPO_4$: In the structure of $PbLiPO_4$, there are two phosphate groups per asymmetric unit and the occupancy factor for the two phosphorus atoms is 1:1.[17] The ^{31}P MAS NMR spectrum (Figure 5) consists of two peaks at 3.5 and 8.1 ppm with an intensity ratio of 1 to 1. We can assign these peaks making use of the proposed inverse correlation between ^{31}P isotropic chemical shift and bond strength.[17] Table II summarizes the summed bond strengths of the oxygen atom belonging to the two PO_4 tetrahedra as calculated from the structure according to Brown and Wu.[19] On the basis of this calculation, we assign the most upfield peak at 3.5 ppm to P(1) and the peak at 8.1 ppm to P(2). The assignment is consistent with the larger chemical shift anisotropy of

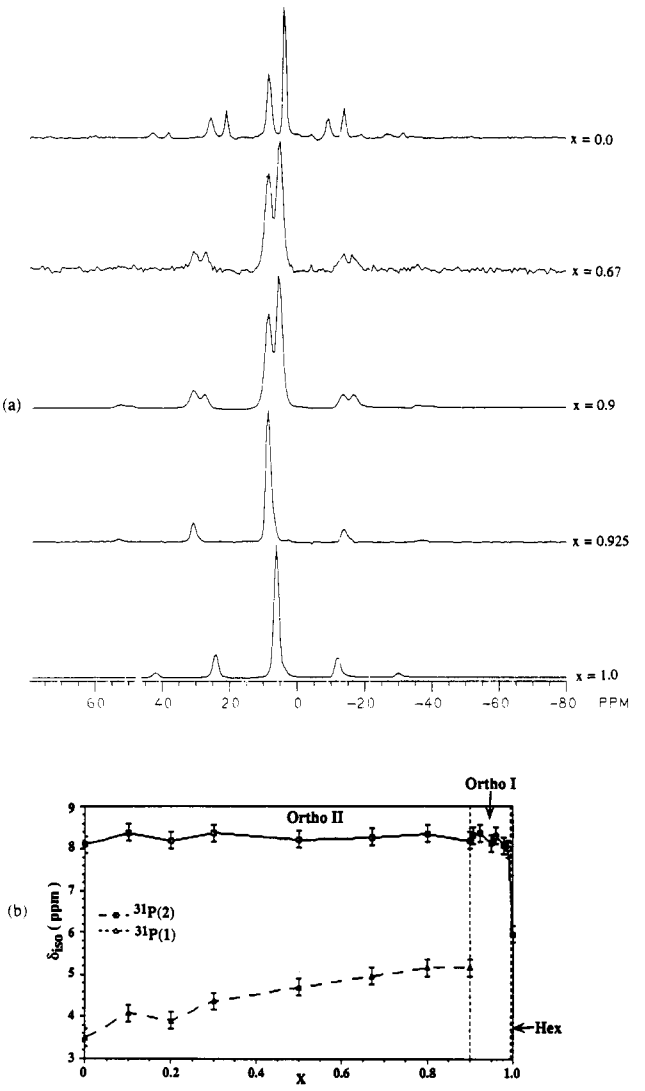

Figure 5. (a) Representative ^{31}P MAS NMR spectra for the $Sr_xPb_{1-x}LiPO_4$ series. (b) Plot of the ^{31}P isotropic chemical shifts relative to 85% H_3PO_4 for the P(2) site (⊡) and the P(1) site (△) vs x for $Sr_xPb_{1-x}LiPO_4$.

Table II. Bond Lengths Given in Elammari et al. and Calculated Bond Valences S According to Brown and Wu[19]

	bond length (Å)	$S(P^{5+})$	$\Sigma S(O^{2-})$
P(1)–O(1)	1.567(9)	1.168	2.047
P(1)–O(2)	1.544(9)	1.224	1.975
P(1)–O(3)	1.525(11)	1.274	2.031
P(1)–O(4)	1.519(9)	1.290	1.903
		sum 4.956	7.956
		range 0.055	0.065
P(2)–O(5)	1.539(10)	1.237	1.962
P(2)–O(6)	1.522(9)	1.282	1.906
P(2)–O(7)	1.600(9)	1.092	1.947
P(2)–O(8)	1.541(9)	1.232	1.840
		sum 4.843	7.655
		range 0.082	0.056

the P(2) site, as is apparent from the more intense spinning sidebands relative to the corresponding centerband. The $PbLiPO_4$ structure reveals indeed that the P(2) tetrahedra are significantly more distorted than the P(1) tetrahedra.[17]

$Sr_xPb_{1-x}LiPO_4$: With increasing Sr substitution the isotropic chemical shift of the 3.5 ppm peak moves downfield (see Figure 5), whereas the resonance at 8.1 ppm is affected very little. At the composition $Sr_{.85}Pb_{.15}LiPO_4$, we observe a main resonance at 8.3 ppm with three shoulders near 10.0, 7.6, and 6.8 ppm. Intensity rear-

(17) Elammari, L.; Elouadi, B.; Depmeier, W. *J. Solid State Chem.* **1988**, *76*, 266.
(18) Cheetham, A. K.; Clayden, N. J.; Dobson, C. M.; Jakeman, R. J. B. *J. Chem. Soc., Chem. Commun.* **1986**, 195.
(19) Brown, I. D.; Wu, K. K. *Acta Crystallogr. Sect. B* **1976**, *32*, 1957.

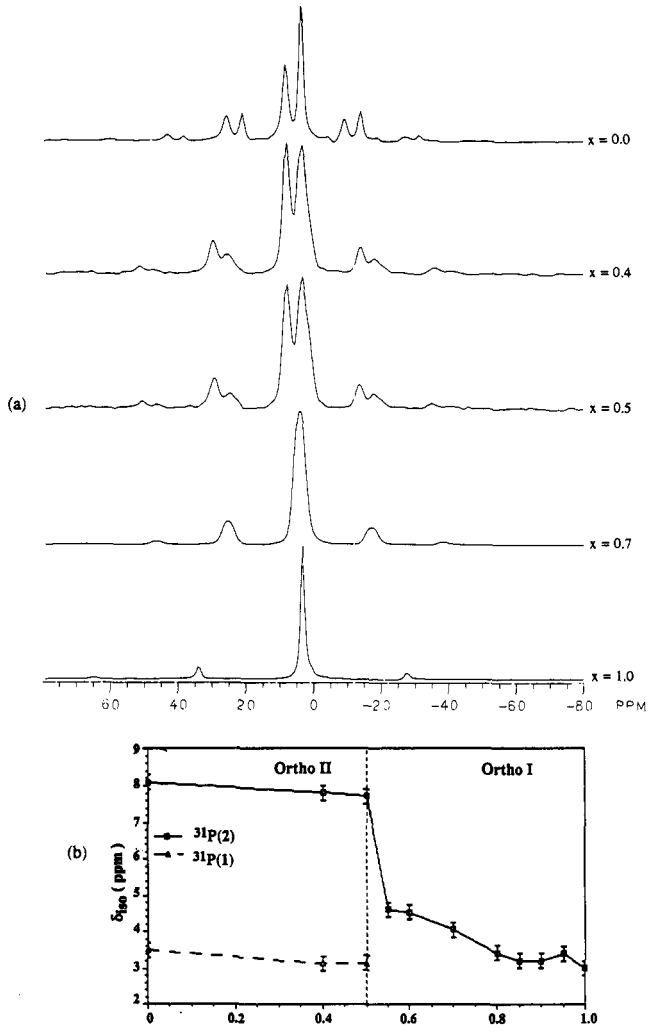

Figure 6. (a) Representative ^{31}P MAS NMR spectra for the $Ba_xPb_{1-x}LiPO_4$ series. (b) Plot of the ^{31}P isotropic chemical shifts relative to 85% H_3PO_4 for the P(2) site (□) and the P(1) site (△) vs x for $Ba_xPb_{1-x}LiPO_4$.

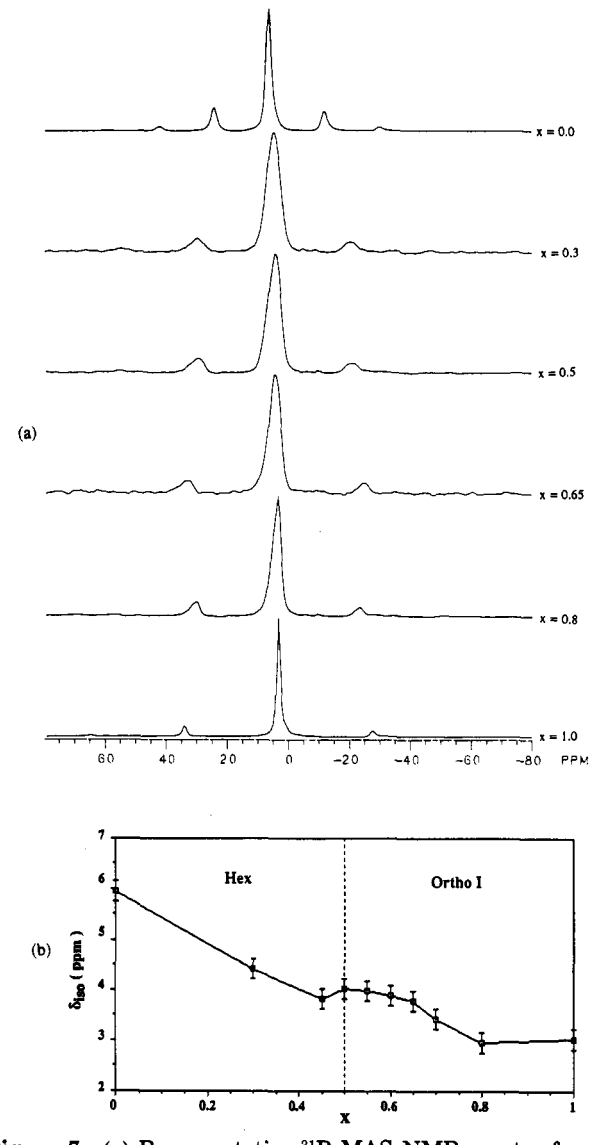

Figure 7. (a) Representative ^{31}P MAS NMR spectra for the $Ba_xSr_{1-x}LiPO_4$ series. (b) Plot of the ^{31}P isotropic chemical shifts (relative to 85% H_3PO_4) vs x for $Ba_xSr_{1-x}LiPO_4$.

rangements in these shoulders continue to $x = 0.9$ where there is only one shoulder at 8.6 ppm besides the main resonance. Above $x = 0.91$, only single-peak spectra are observed as the structure changes from the $PbLiPO_4$ structure to a new orthorhombic phase where both phosphorus atoms become equivalent. Finally, the transition to hexagonal at $x = 0.99$ (Figure 5b) is reflected in the abrupt chemical shift change from 8.1 to 6.0 ppm, the only single site in $SrLiPO_4$.

$Ba_xPb_{1-x}LiPO_4$: Substitution of Pb by Ba into the $PbLiPO_4$ structure results in an uniform decrease in chemical shift for both the P(1) and P(2) sites. It appears that in contrast to the $Sr_xPb_{1-x}LiPO_4$ solid solution both sites are affected equally by the substitution. Beyond the phase transition, there is only a single site which shifts monotonically upfield with increasing Ba substitution (Figure 6).

$Ba_xSr_{1-x}LiPO_4$: Both the pure $BaLiPO_4$ and $SrLiPO_4$ have single phosphorus atom sites and the ^{31}P MAS NMR isotropic chemical shifts are at 3.0 and 6.0 ppm respectively. With increasing x, the NMR spectra appear to consist of closely spaced multiple lines, indicating the presence of local P environments with differing numbers of nearby Ba and Sr atoms (Figure 7). As observed in the other systems, the peaks move upfield with increasing Ba content. There appears to be no distinct chemical shift discontinuity at the phase transition hence confirming its displacive nature.

Optical Responses. *SHG.* $Ba_xPb_{1-x}LiPO_4$: The powder SHG of pure $PbLiPO_4$ and $BaLiPO_4$ are respectively, 37 ± 10% and 10 ± 10% times that of quartz. The SHG values increase upon doping the system with barium and maximize close to the structural phase transition at $Ba_{0.55}Pb_{0.45}LiPO_4$ (486 ± 10%), then decrease drastically with higher barium content (Figure 2).

$Sr_xPb_{1-x}LiPO_4$: Pure $SrLiPO_4$ has a SHG value of 9 ± 10% times that of quartz. Upon doping the pure strontium phase with lead, the SHG increases and maximizes at $x = 0.925$ with a value of 120 ± 10% (Figure 3). This may be due to the fact that there is a phase transition around $x = 0.9$. Upon further doping of lead, the SHG stays relatively constant.

$Ba_xSr_{1-x}LiPO_4$: The SHG of $SrLiPO_4$ increases monotonically upon addition of barium. Beyond the phase transition ($x = 0.5$), the SHG value continues to increase until it reaches a maximum at $Ba_{0.9}Sr_{0.1}LiPO_4$ (81 ± 10%), then decreases rapidly upon higher loading of barium (Figure 4). Close to the phase transition, formation of the two phased materials was avoided using the cooling method

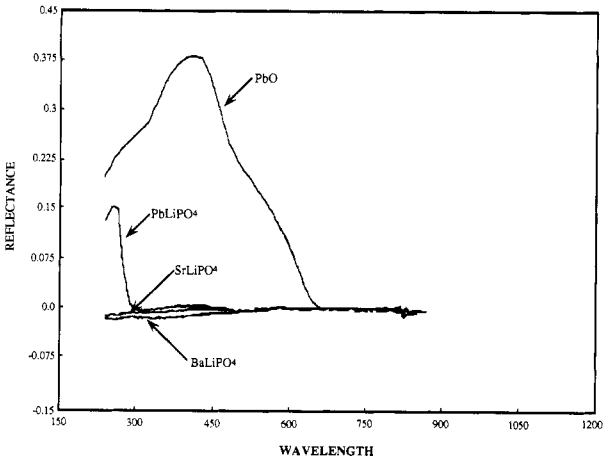

Figure 8. Vis/UV absorption spectra for both $BaLiPO_4$, $SrLiPO_4$, and $PbLiPO_4$ along with the vis/UV spectrum of PbO taken from 850 to 220 nm. The absorption edge for $BaLiPO_4$ and $SrLiPO_4$ are below 220 nm.

Table III. Vis/UV Absorption Edges of Representative Compounds from the $Sr_xPb_{1-x}LiPO_4$ and $Ba_xPb_{1-x}LiPO_4$ Series Measured against $MgCO_3$

material	vis/UV (±2 nm)	material	vis/UV (±2 nm)
$PbLiPO_4$	271	$Ba_{0.2}Pb_{0.8}LiPO_4$	271
$Sr_{0.67}Pb_{0.33}LiPO_4$	262	$Ba_{0.525}Pb_{0.475}LiPO_4$	262
$Sr_{0.91}Pb_{0.09}LiPO_4$	244	$Ba_{0.9}Pb_{0.1}LiPO_4$	264
$Sr_{0.925}Pb_{0.075}LiPO_4$	253	$Ba_{0.9}Pb_{0.1}LiPO_4$	264
$Sr_{0.96}Pb_{0.04}LiPO_4$	<220	$BaLiPO_4$	<220
$Sr_{0.98}Pb_{0.02}LiPO_4$	<220		
$SrLiPO_4$	<220		

[a] The spectra were taken from 850 to 220 nm.

described in the experimental section. By either slowly cooling these compounds to room temperature or quenching them in liquid nitrogen, it was possible to obtain phase-pure materials. For both slow and fast cooled samples of the same composition and phase, there was no change in the SHG value to within the 10% error range.

Vis/UV Spectroscopy. $SrLiPO_4$, $BaLiPO_4$, and their solid solutions are transparent in the vis/UV over the entire range investigated. Figure 8 shows the spectra of $SrLiPO_4$, $BaLiPO_4$, $PbLiPO_4$, and PbO. For pure $PbLiPO_4$ the absorption edge is found to be at 271 ± 2 nm, and as Ba is doped into the $PbLiPO_4$ structure, the absorption edge shifts toward the ultraviolet region. For $Sr_xPb_{1-x}LiPO_4$ the absorption edge shifts from 271 ± 2 nm in pure $PbLiPO_4$ to 253 ± 2 nm up to $x = 0.925$, upon even higher Sr doping the absorption edge begins to resemble that of $SrLiPO_4$ (Table III).

Raman Spectroscopy. The Raman spectra of both $PbLiPO_4$ and $BaLiPO_4$ match those taken by Paques-Ledent,[20] and the peak assignment is done by utilizing the arguments given there. However, the X-ray powder pattern of $SrLiPO_4$ presented in Paques-Ledent et al. is monoclinic which is different from what we have found. From our X-ray data, we propose for $SrLiPO_4$ a hexagonal structure similar to that of $KLiSO_4$ (phase I or II)[21] with alternate "up" and "down" LiO_4 (or SO_4) tetrahedra. The Raman spectrum of the hexagonal $SrLiPO_4$ is a simpler version of the orthorhombic $BaLiPO_4$ spectrum. By

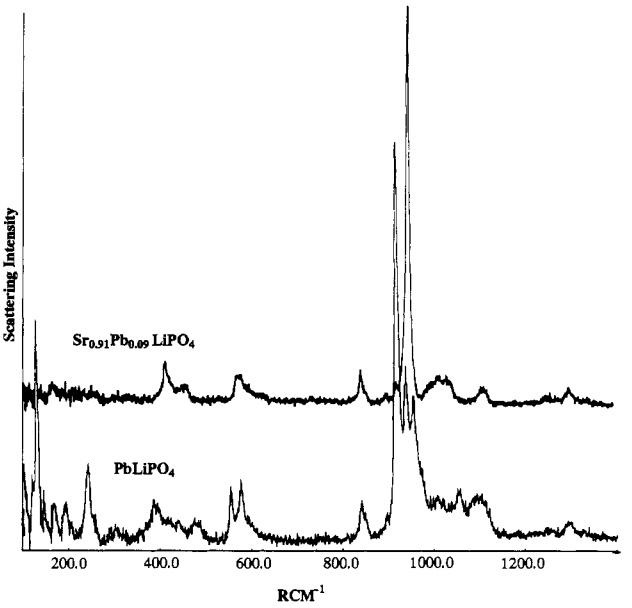

Figure 9. Raman spectra of (a) $PbLiPO_4$ and (b) $Sr_{0.98}Pb_{0.02}LiPO_4$ using an argon 514-nm continuous-wave ion laser. The samples were scanned between 100 and 1400 cm^{-1}.

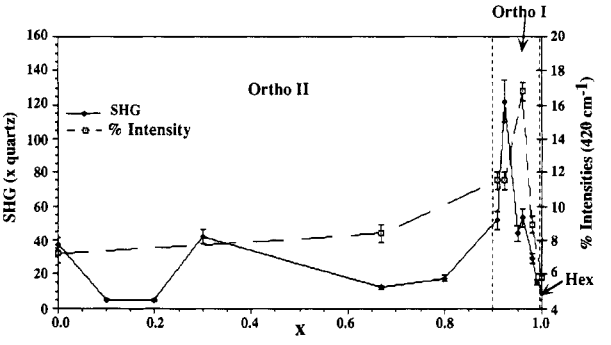

Figure 10. SHG (□) and ratio of Raman scattering intensity of the 420 cm^{-1} band to the $\nu_1(PO_4)$ mode (♦) vs x for $Sr_xPb_{1-x}LiPO_4$.

comparing spectra from the $Sr_xPb_{1-x}LiPO_4$ and $Ba_xSr_{1-x}LiPO_4$ series, we were able to follow the intensity changes for each peak.

In the $Sr_xPb_{1-x}LiPO_4$ series ($0.91 \leq x \leq 1.00$), the symmetric stretching P–O, $\nu_1(PO_4)$ mode is observed at 946 ± 2 cm^{-1}. In $PbLiPO_4$, the totally symmetric stretching modes belonging to the two PO_4 tetrahedra are well resolved at 924 and 959 cm^{-1}. Figure 9 shows representative spectra in the system $Sr_xPb_{1-x}LiPO_4$. With increasing x, the peaks at 924 and 959 cm^{-1} broaden and eventually disappear while the intensity of the peak at 944 cm^{-1} increases. Figure 10 compares the intensity ratio of the Raman band at ~420 cm^{-1} to that of the $\nu_1(PO_4)$ mode with the SHG values as a function of composition in the system $Sr_xPb_{1-x}LiPO_4$. Anomalies are apparent in both parameters, particularly near the phase transitions, although not necessarily for the same sample. A similar correlation is found for the internal Li–O vibration of $Sr_xPb_{1-x}LiPO_4$ and $Ba_xPb_{1-x}LiPO_4$.

A 1:1 correlation between SHG and Raman intensities is not expected due to the fact that all the structural and electronic components relate to second harmonic generation whereas Raman spectroscopy measures the normal modes of individual bonds. In particular we expect that the intensities of the Pb–O bond vibrations observed in the Raman spectra also contribute to second harmonic

(20) Paques-Ledent, M. *J. Solid State Chem.* **1978**, *23*, 155.
(21) Fujimoto, S.; Yasuda, N.; Hibino, H. *J. Phys. D: Appl. Phys.* **1985**, *18*, L135.
(22) Bussman, A., Biltz, H. *Ferroelectrics* **1980**, *25*, 343.

generation, however we were not able to observe the low-frequency Pb–O vibrations.

Conclusion

The charge asymmetry inherently introduced by using large and small cations in the $ABCO_4$ structures produces a significant SHG response permitted by the crystal symmetry. As relatives of the stuffed tridymite structures these are also comparatively low oxygen density phases. More importantly, our synthesis studies of $MLiPO_4$ (M = Sr, Ba, Pb) have shown that the SHG of these materials can be maximized by bringing each system close to its structural phase transition. From the ^{31}P MAS NMR and X-ray studies of the doped systems, we have found that the more drastic the phase transition the higher the SHG. This is demonstrated by the $Ba_xSr_{1-x}LiPO_4$ series where the transition is displacive, so that there is relatively small change in the SHG compared to either the $Ba_xPb_{1-x}LiPO_4$ or $Sr_xPb_{1-x}LiPO_4$ systems where the rearrangement of atoms close to the phase transition involved bond breaking. It should be noted that the observed SHG response is the consequence of changes in both linear and nonlinear components of the optical susceptibility.

The vis/UV data show that these materials are transparent in the UV region to 271 nm. From Raman spectroscopic data, we have found a correlation between the second harmonic generation and Raman intensities. The maximum intensity of Raman scattering at $\sim 398\ cm^{-1}$ (symmetric bending modes of PO_4) follow the general trend of the increase in SHG observed in the orthorhombic I phase.

SHG close to the structural phase transition is as much as 486 times quartz. This response is substantially greater than the currently available UV transparent frequency doubling β-BaB_2O_4. We are presently growing single crystals of $ABCO_4$ materials which exhibit polycrystalline SHG responses which are greater than 100 times that of quartz.

Acknowledgment. The authors are grateful to Dr. Vojislav Srdanov for setting up the SHG apparatus, Tamara Bloomer of UCSB Engineering Materials for the SEM data and help with particle size measurements, and the group of John Bierlein at DuPont for some of the SHG measurements presented in Table I. This work is supported by the National Science Foundation Division of Material Research, under DMR 9208511.